

Resistance to 2,3,7,8-Tetrachlorodibenzo-*p*-dioxin Toxicity and Abnormal Liver Development in Mice Carrying a Mutation in the Nuclear Localization Sequence of the Aryl Hydrocarbon Receptor*

Received for publication, September 18, 2002, and in revised form, February 27, 2003
Published, JBC Papers in Press, March 5, 2003, DOI 10.1074/jbc.M209594200

Maureen K. Bunker^{‡§}, Susan M. Moran[‡], Edward Glover[‡], Tami L. Thomae[‡], Gareth P. Lahvis[‡],
Bernice C. Lin[‡], and Christopher A. Bradfield^{‡¶}

From the [‡]McArdle Laboratory for Cancer Research and the [§]Training Program in Environmental Toxicology, University of Wisconsin Medical School, Madison, Wisconsin 53706

The Ah receptor (AHR) mediates the metabolic adaptation to a number of planar aromatic chemicals. Essential steps in this adaptive mechanism include AHR binding of ligand in the cytosol, translocation of the receptor to the nucleus, dimerization with the Ah receptor nuclear translocator, and binding of this heterodimeric transcription factor to dioxin-responsive elements (DREs) upstream of promoters that regulate the expression of genes involved in xenobiotic metabolism. The AHR is also involved in other aspects of mammalian biology, such as the toxicity of molecules like 2,3,7,8-tetrachlorodibenzo-*p*-dioxin as well as regulation of normal liver development. In an effort to test whether these additional AHR-mediated processes require a nuclear event, such as DRE binding, we used homologous recombination to generate mice with a mutation in the AHR nuclear localization/DRE binding domain. These *Ahr*^{nls} mice were found to be resistant to all 2,3,7,8-tetrachlorodibenzo-*p*-dioxin-induced toxic responses that we examined, including hepatomegaly, thymic involution, and cleft palate formation. Moreover, aberrations in liver development observed in these mice were identical to that observed in mice harboring a null allele at the *Ahr* locus. Taken in sum, these data support a model where most, if not all, of AHR-regulated biology requires nuclear localization.

years, the mechanistic details of this adaptive signaling pathway have been well characterized (1–4). The AHR is a basic helix-loop-helix-PAS (bHLH-PAS) transcription factor. Upon binding agonists, the AHR translocates from the cytoplasm to the nucleus, where it forms a heterodimer with another bHLH-PAS protein known as the aryl hydrocarbon nuclear translocator (ARNT). This heterodimeric complex interacts with dioxin-responsive elements (DREs) within the genome and up-regulates the transcription of a battery of xenobiotic metabolizing enzymes (XMEs). These regulated XMEs include the cytochrome P450s *Cyp1a1*, *Cyp1b1*, and *Cyp1a2* and the phase II enzymes *Gst-a1* and *Ugt1-06* (reviewed in Refs. 2 and 3).

In addition to regulating an adaptive metabolic response, the AHR also mediates toxic responses to 2,3,7,8-tetrachlorodibenzo-*p*-dioxin (TCDD) and plays an important role in normal development. Early genetic and pharmacological experiments provided evidence that the AHR mediates toxic responses to TCDD and related pollutants (5). Highly reproducible toxic endpoints in rodent species include thymic involution, hepatomegaly, epithelial hyperplasia, and teratogenesis. More recently, generation of null alleles at the *Ahr* locus in mice revealed that the AHR also plays an important role in normal mammalian development (6–9). Across laboratories, the most reproducible phenotype associated with the homozygous null allele is a smaller liver. We have proposed that smaller liver size is the result of the persistence of a fetal vascular structure known as the ductus venosus (DV) (10). Our hypothesis is that smaller liver size is due to hepatocyte atrophy, resulting from partial shunting of portal blood flow directly to the vena cava. Importantly, the mechanistic role of AHR in the persistence of the DV as well as the appearance of other vascular aberrations is unknown.

Our laboratory is interested in determining if the adaptive, toxic, and developmental pathways of AHR differ in any mechanistic aspect. In particular, we are interested in understanding whether cytosolic events, nuclear events, or DRE-mediated transcription play a role in TCDD-induced toxicity or in the establishment of a normal liver size. Although it may be assumed that all actions of AHR are dependent upon DRE-mediated transcription, a considerable body of evidence has been reported to the contrary. In this regard, signal transduction through cellular factors such as the cSrc kinase, the retinoblastoma protein (Rb), ceramide, steroid receptors, NF- κ B, and HIF1 α has been reported to be modulated by AHR agonists in a manner that is independent of AHR DRE binding and transcriptional activation roles (11–17).

In an effort to formally examine the possibility that aspects of AHR biology are mediated through cytosolic events that do not require the AHR to translocate to the nuclear compart-

The aryl hydrocarbon receptor (AHR)¹ regulates an adaptive metabolic response to a variety of planar aromatic chemicals that are widely dispersed in the environment. Over the last 20

* This work was supported by National Institutes of Health Grants P01-CA22484, P30-CA07175–CA14520, T32-CA09135, T32-ES07015, and F32-ES05877 and a fellowship from the Mary Engsborg Fund. The costs of publication of this article were defrayed in part by the payment of page charges. This article must therefore be hereby marked “advertisement” in accordance with 18 U.S.C. Section 1734 solely to indicate this fact.

[¶] To whom correspondence should be addressed: McArdle Laboratory for Cancer Research, 1400 University Ave., Madison, WI 53706. Tel.: 608-262-2024; Fax: 608-262-2824; E-mail: bradfield@oncology.wisc.edu.

¹ The abbreviations used are: AHR, aryl hydrocarbon receptor; *Ahr*^{nls}, the *Ahr* nls allele generated; AHR^{nls}, the AHR^{nls} protein that arises from the mutant allele; ARNT, aryl hydrocarbon receptor nuclear translocator; BEAR, bacterially expressed aryl hydrocarbon receptor; bHLH, basic helix-loop-helix; β NF, β -naphthoflavone; dpm, disintegrations/min; DRE, dioxin response element; DV, ductous venosus; EROD, ethoxyresorufin-*o*-de-ethylase; ES, embryonic stem; HSP90, 90-kDa heat shock protein; NLS, nuclear localization signal; PAS, Period-ARNT-Singleminded; Rb, retinoblastoma; TCDD, 2,3,7,8-tetrachlorodibenzo-*p*-dioxin; XME, xenobiotic metabolizing enzyme; MOPS, 4-morpholinepropanesulfonic acid; [¹²⁵I]Br2DpD, 2-azido-3-iodo[¹²⁵I]iodo-7,8-dibromodibenzo-*p*-dioxin; IVC, inferior vena cava.

ment, we undertook the approach of using gene targeting in mouse embryonic stem (ES) cells to generate a novel allele at *Ahr* that harbors a mutation that blocks both nuclear localization and DRE binding (designated as *Ahr^{nls}*). By examining the responses of these mutant animals to TCDD and through a comparison with other *Ahr* alleles, we are able to define the relative importance of cytosolic *versus* nuclear events in various aspects of AHR biology.

EXPERIMENTAL PROCEDURES

Strategy—The design of the AHR^{nls} allele (and therefore the *Ahr^{nls}* protein) is based on published results from several laboratories as well as practical considerations. Foremost is the observation that the residues required for DRE binding overlap with those required for nuclear localization. Previous mutational analysis reveals that the AHR nuclear localization sequence (NLS) is bipartite and resides within the basic region residues 12–17 and 37–42 (18–20). These regions significantly overlap with those shown to be critical for DRE binding, including residues 9–14 and 36–39 (21–23) (Fig. 1A). Because of this domain overlap, we chose to introduce a series of nonconservative mutations to change Arg³⁷, His³⁸, and Arg³⁹ to Ala³⁷, Gly³⁸, and Ser³⁹, respectively. Our prediction was that this would generate an AHR protein that is deficient in both nuclear localization and DRE binding. Based upon the work cited above and our previous domain mapping work, we predicted that these mutations would not influence ligand binding, chaperone binding, or dimerization with ARNT (24).

Oligonucleotides—Oligonucleotides (Invitrogen) are designated as follows: OL72, 5'-GGTTCGAATTTCCAGGATG-3'; OL73, 5'-TCGAGTAGATCAGCAATGGGCCAGC-3'; OL74, 5'-TCGAGCTGGGCCCA-TTGCCTGATCTAC-3'; OL659, 5'-ATCCAGAAGAGCTTATCAGTGGT-CTGCG-3'; OL941, 5'-CTGAGGGGACGTTTAAATG-3'; OL942, 5'-AACATTTGCACTCATGGATAG-3'; OL975, 5'-GCGTCGACCCACATG-AGCAGCGGCCCAACATC-3'; OL1352, 5'-GGTACCTCTGAGTTCA-AGTCTAGTCTG-3'; OL1353, 5'-GGTACCGCATGCTTACTAGTAGTT-TTCTAG-3'; OL1503, 5'-GCCACATGAGCAGCGGCCCAACATC-ACCTATGCCAGCCGCAAGCGGCCAA GCGGTCGAGAAAACAG-TAAAGCCCGGGCCGCTGAA-3'; OL1500, 5'-GTAAGCCCGGGCC-CGCTGAAGGAATTAAGTCAAATCCTTCTAA GGCAGGATCCGACC-GGCTGAACACAGAGTTAGA-3'; OL2639, 5'-ACTAGTCGACCTAA-CCCATTGCTGTCCACCAGTCATGCTAGCCATACTCTGCACCTTG-CTTAG-3'.

Expression Constructs—The construct pSV-AHR (PL 65) is previously described (25, 26). To construct pTgTAHRT7 (PL1550), PL65 was used as a template for 22 rounds of PCR amplification using OL1503 (forward) and OL2639 (reverse) as primers. The resulting amplicon was cloned into the pTarget™ mammalian expression vector (Promega, Madison, WI). OL1503 contains a consensus Kozak start codon and a conservative mutation creating an *SrfI* site to match the targeting construct sequence (see below). The oligonucleotide OL2639 contains the region of AHR cDNA preceding the stop codon, followed by sequences for the T7 epitope and for a translational stop codon. The plasmid pSVAHR^{nls} (PL1108) was made by three-step PCR using PL65 as template. In the first step, the forward oligonucleotide, OL1500, containing a 9-base substitution that changed codons Arg³⁷ to Ala³⁷, His³⁸ to Gly³⁸, and Arg³⁹ to Ser³⁹, respectively, was used in a PCR-amplification with the reverse oligonucleotide OL72. The product was then used as template for 20 rounds of amplification using OL1503 and OL72 to add the 5' amino acids. This product was then amplified using OL975 and OL72 to add a consensus Kozak start codon for increased expression. An *SpeI/NaeI* fragment was excised and used to replace the *SpeI/NaeI* fragment from PL65 to create pSVAHR^{nls} (PL1108). Sequencing of the full-length constructs ensured that no other mutations were present.

Protein Analysis—Gel shifts and coimmunoprecipitations were performed as described previously (16, 27, 28). *In vitro* protein expression was carried out using the TNT® coupled transcription/translation reticulocyte lysate system (Promega). For gel shift assays, *in vitro* expressed proteins were incubated with a ³²P-labeled DRE fragment derived from annealing OL73 and OL74 in the presence or absence of 10 μM β-naphthoflavone (βNF). The presence of the AHR in the DRE binding complex was confirmed using a high affinity rabbit polyclonal antibody raised against recombinant AHR (BEAR-3). Co-immunoprecipitation experiments were performed by co-incubating ~10 fmol of reticulocyte lysate-expressed proteins with 2 μg of antibody in 500 μl of cold MENG buffer (25 mM MOPS, pH 7.5, 0.025% sodium azide, 1 mM EGTA, 10% glycerol, pH 7.5), supplemented with 15 mM NaCl, 0.1 mM

dithiothreitol, and 0.1% Nonidet P-40. Bound protein-antibody complexes were precipitated with protein A-Sepharose (Sigma) for 1.5 h at 4 °C, washed four times with cold MENG buffer, eluted in 2× SDS sample buffer, and analyzed by SDS-PAGE.

Western blots, EROD assays, and photoaffinity labeling of the AHR were performed using methods described previously (7, 29, 31). Microsomal and cytosolic fractions were isolated from ~0.5 g of mouse liver that was homogenized in ice-cold MENG buffer followed by two high speed centrifugations at 10,000 × *g* and 100,000 × *g*. The microsomal pellet was resuspended in 1 ml of resuspension buffer (15 mM Tris-Cl, pH 8.0, 250 mM sucrose). The supernatant, containing cytosolic protein, was saved for later AHR analysis. Western blot analysis was performed as described using the BEAR-3 antibody and a secondary antibody labeled with alkaline phosphatase (29). The EROD assays were performed in a 96-well format. In each well, one-one thousandth of the total microsomal preparation was diluted into 200 μl in MENG buffer. To start the reaction, 3 μl of 0.1 mM 7-ethoxyresorufin and 20 μl of 5 mM NADPH were added. The production of 7-hydroxyresorufin was measured by fluorometry (*fMax*; Molecular Devices) at excitation of 510 nm, emission of 590 nm every 30 s over 10 min at 25 °C. Total protein concentration was determined using the BCA assay (Pierce). The results are expressed as relative fluorescence units/min as calculated using SoftMaxPro software (Molecular Devices) and normalized to total protein levels. Photoaffinity labeling of the AHR protein with 2-azido-3-iodo[¹²⁵I]iodo-7,8-dibromodibenzo-*p*-dioxin ([¹²⁵I]Br2DpD) was performed essentially as described (31). Briefly, for labeling of the cytosolic AHR, liver cytosolic protein (300 μg/ml) was incubated with [¹²⁵I]Br2DpD at the indicated concentrations for 2 h at 4 °C. This was followed by the addition of one-tenth volume of 1%/0.1% activated charcoal/gelatin for 30 min at 4 °C to remove unbound ligand. Following centrifugation, supernatants were exposed to UV light at 310 nm (80 watts, 4 cm) for 30 s. Protein was precipitated in acetone and separated by 7.5% SDS-PAGE. The location of labeled receptor was determined by autoradiography, and the band was excised and counted by γ emissions. The quantity of bound ligand is expressed as dpm/lane. The *in vitro* translated proteins were labeled by diluting 10 μl of the translation reaction in 0.5 ml of MENG. We ensured that the 10 μl of translation reaction contained equal amounts of translated receptor by ³⁵S calibration. The receptor was then labeled with 1 nM [¹²⁵I]Br2DpD for 30 min at 20 °C followed by 4 °C for 5 min. Unbound ligand was removed by charcoal/gelatin, and the quantity of bound ligand was determined in the same manner as above. The specific activity of the radioligand is 2176 Ci/mmol, and 1 pmol = 4,830,700 dpm. For Scatchard analysis, it was assumed that free probe was equal to total counts added and that total bound was equal to specific bound (this assumes that nonspecific binding is negligible following SDS-PAGE and band excision) (30).

Cell Culture Conditions—ES cells, designated GS-1, were purchased from Genome Systems (St. Louis, MO). The ES cells were cultured on a confluent layer of Mitomycin-c-treated mouse embryonic fibroblasts derived from PGK-NeoR transgenic mice (formal designation C57BL/6-TgN(PGKneoBpA)3Ems; Jackson Laboratory, Bar Harbor, ME) in Dulbecco's modified Eagle's medium-high glucose supplemented with 20% fetal bovine serum (Hyclone, Logan, UT), 0.1 mM nonessential amino acids, 2 mM L-glutamine, 10 mM HEPES, 100 units/ml penicillin, 100 μg/ml streptomycin, and 1000 units/ml ESGRO™ (Invitrogen).

Generation of Mouse Embryonic Fibroblasts—We have previously generated *Ahr* null mice that will be hereafter referred to as *Ahr*^{-/-} (formal genetic designation is *Ahr^{tmBra1}*). To generate matched mouse embryonic fibroblasts, *Ahr*^{+/-} mice that have been backcrossed to C57BL/6 for 16 generations were intercrossed to generate littermate +/+, +/-, and -/- embryos. Embryos were isolated from their yolk sacs, and heads and livers were removed by dissection. DNA was isolated from the heads of individual embryos and was used for genotyping as described (10). At passage 2 (P2), *Ahr*^{+/+} and *Ahr*^{-/-} fibroblasts were maintained on a "3T3 protocol" until passage 25 and then passaged regularly at subconfluence as described (32). Briefly, in the 3T3 protocol, cells were grown in 6-cm dishes in Dulbecco's modified Eagle's medium-high glucose, supplemented with 10% fetal bovine serum, 0.1 mM nonessential amino acids, 2 mM L-glutamine, 10 mM HEPES, 100 units/ml penicillin, and 100 μg/ml streptomycin. Every 3rd day, cells were trypsinized and replated at a density of 3 × 10⁵. At passage 28, individual clones were isolated from one line of each genotype and passaged regularly at subconfluence. The *Ahr*^{-/-} subcloned cell line used for these experiments was designated B4.4.

Transfection of Mouse Embryonic Fibroblasts—Transient transfections of mouse embryonic fibroblasts were performed using Fugene6 reagent (Roche Applied Sciences) with 1 μg of total DNA and a 3:1 Fugene6/DNA ratio. When TCDD was used, cells were allowed to re-

cover for 1 day after transfection. Following this period, 1 nM TCDD was added directly to the medium in Me₂SO (final Me₂SO concentration 0.1%) and cells were harvested after 2 h. Immunofluorescence was performed as described (26) using BEAR-3 and a fluorescein isothiocyanate-conjugated goat anti-rabbit secondary antibody (Jackson ImmunoResearch, West Grove, PA) for fluorescence detection.

Generation of Ahr^{nls/nls} Mice—A 15-kb region of homology surrounding exon 2 of AHR was isolated from a 129SvJ genomic library (Genome Systems) as described (7, 33). To make the Ahr^{nls} allele, a 9-nucleotide replacement was introduced by using the PCR product of OL1500 and OL942 as megaprimer with 22 rounds of amplification with OL941 (23). The *Sph*I fragment from the mutant PCR product was used to replace exon 2 in an 8-kb *Bam*HI genomic fragment. A 5.5-kb region containing the mutated exon 2 was amplified with OL1352 and OL1353 and cloned into the *Kpn*I site of ploxPNT (34). A 7-kb *Sph*I fragment from the 5' region of exon 2 was cloned into the *Not*I/*Xho*I site of this construct to make the final targeting construct that was designated pNTAHRnls (PL1075). For homologous recombination in ES cells, ~10 μg of targeting construct was electroporated into GS1 cells (Genome Systems), and selection was performed using 200 μg/ml G418 and 1 mM Ganciclovir. Clones were screened by Southern blot of *Bam*HI-digested genomic DNA using a probe 3' to the end of the targeting construct (PL311). Correctly targeted clones were injected into 3.5-day postcoital C57BL/6 blastocysts, and resulting chimeras were backcrossed to C57BL/6 to determine contribution of the ES clones to the germ line. For experimental analysis, animals were backcrossed to C57BL/6 mice that are congenic for the Ahr^d allele (35). Mice were genotyped using the PCR primers OL941 and OL942. The PCR was carried out for 35 cycles (95 °C, 1 min; 63 °C, 1 min; 72 °C, 1 min) in buffer containing 4 mM MgCl₂; a *Bam*HI digest cuts the 380-bp PCR product from the Ahr^{nls} allele into two small fragments of 240 and 140 bp that were detected on a 2% agarose gel.

Animals—Animals were housed in a selective pathogen-free facility on corn cob bedding with food and water *ad libitum* according to the rules and guidelines set by the University of Wisconsin. When TCDD was used, 5-week-old animals were injected once intraperitoneally with 100 μg/kg TCDD in *p*-dioxane or with *p*-dioxane alone. After 6 days, animals were weighed and sacrificed, and organs were immediately removed and weighed. For angiography, ~1 ml of Omnipaque 300 (Nycomed, Inc., Princeton, NJ) was injected into the hepatic portal vein postmortem. Continuous x-ray images were obtained over ~10 s using an OEC 9800 Portable Vascular C-ARM (Medical Systems, Inc., Salt Lake City, UT).

In order to directly compare the null, wild type, and Ahr^{nls/nls} alleles, genetic background had to be taken into consideration. Mice used in these experiments that are defined as harboring the Ahr⁻ allele have been previously backcrossed to C57BL/6 for 16 generations. Because C57BL/6 carries the high affinity Ahr^b allele and the Ahr^{nls} allele was created in 129 ES cells carrying the lower affinity Ahr^d allele, we used a C57BL/6 strain congenic for DBA2-derived Ahr^d allele to make subsequent backcrosses of both the Ahr⁻ and Ahr^{nls} alleles (generous gift from Alan Poland). This breeding generated wild type Ahr^d allele controls on the C57BL/6 background (35). For clearer presentation, the wild type Ahr^d allele is referred to as Ahr⁺ ("wild type") throughout this paper. Mice harboring the Ahr^{nls} allele were backcrossed for three generations to C57BL/6. To further minimize the influence of genetic background, all experiments were repeated from multiple independently derived sublines. Only a single representative experiment is presented.

Palate Cultures—Suspended palate organ cultures were performed essentially as described (36, 37). Palatal shelves were dissected from embryonic day 12.5 embryos of the Ahr^{+/+}, Ahr^{+/-}, and Ahr^{nls/nls} genotypes. The palates were placed into cold phosphate-buffered saline and then transferred to prewarmed 1:1 Dulbecco's modified Eagle's medium/F-12 medium supplemented with 1% L-glutamine, 1% ascorbate, and 1% penicillin/streptomycin and immediately treated with either 0.03% Me₂SO or 3.3 nM TCDD in 0.033% Me₂SO (*v/v*). After exposure for 4 days, the palates were fixed in 10% formalin and stained with hematoxylin for visualization. Palates were scored as not fused or fused. Ambiguous partially fused palates accounted for only a small percentage and were not included in the data set.

Statistics—In the situation where multiple comparisons could be made, an analysis of variance was performed, and Tukey's test was used to determine differences with a *p* ≤ 0.05 (38). When only two groups were being compared, a two-tailed *t* test was performed with the level of significance set at *p* ≤ 0.05 (Fig. 5) (38).

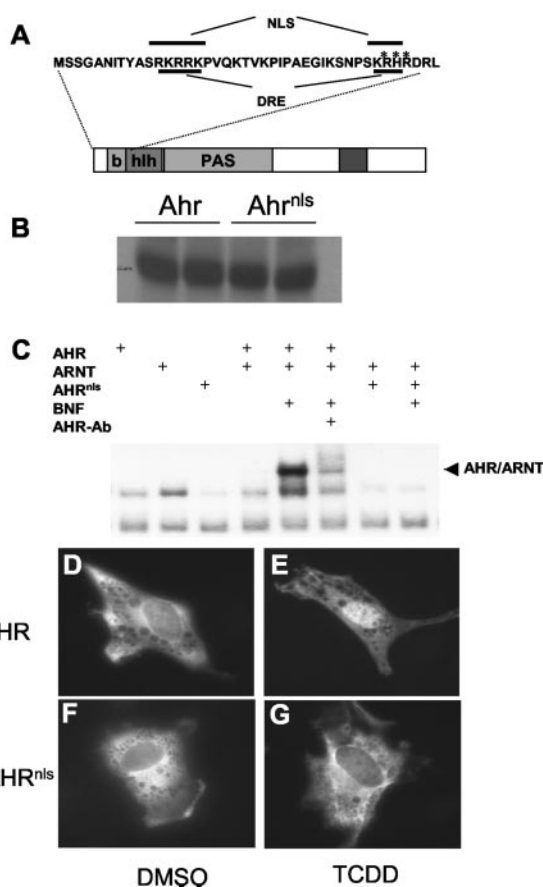


FIG. 1. *In vitro* characterization of AHR^{nls} recombinant protein. A, schematic of AHR protein domain structure. Amino acids 1–43 are depicted. Bars above and below show locations of basic residues involved in nuclear localization (NLS) and DRE binding (DRE). The mutated amino acids in the AHR^{nls} recombinant protein (Arg³⁷, His³⁸, and Arg³⁹) are marked with asterisks. B, photoaffinity labeling of wild-type and Ahr^{nls} recombinant proteins. Recombinant proteins were labeled with [¹²⁵I]Br₂DpD and activated at 310-nm light (described under "Experimental Procedures"). Labeled proteins were separated by PAGE and visualized by autoradiography. A representative experiment with duplicate samples is shown. C, gel shift analysis of AHR, ARNT, and AHR^{nls} recombinant proteins. Recombinant proteins were expressed alone or in the presence of ARNT or ARNT + βNF and analyzed for binding to a ³²P-labeled oligonucleotide with a single DRE element by nondenaturing PAGE. The anti-AHR antibody (AHR-Ab) was added to indicated reaction to block formation of the complex. D–G, subcellular localization of recombinant AHR and AHR^{nls} proteins. Ahr^{-/-} cells were transiently transfected with either AHR (D and E) or AHR^{nls} (F and G) cDNA (pSV-AHR and pSV-AHR^{nls}, respectively). Cells were treated with either 1% Me₂SO (C and E) or 1 nM TCDD plus 1% Me₂SO (D and F), fixed in cold methanol, and analyzed for localization of AHR using anti-AHR antibody and detected with fluorescein isothiocyanate-conjugated secondary antibody. Digital images were collected by standard fluorescence microscopy.

RESULTS

Preliminary Characterization of the Ahr^{nls} Mutation *In Vitro*—In order to generate an AHR protein deficient in nuclear localization, we replaced amino acids Arg³⁷, His³⁸, and Arg³⁹ in the mouse AHR cDNA (pSV-AHR) with nonconservative amino acids Ala, Gly, and Ser, respectively, to generate the plasmid pSV-AHR^{nls} (Fig. 1A). Given the overlap between the NLS and the DRE recognition sequences, this mutant was also predicted to have deficiencies in DRE binding. As a preliminary examination of the characteristics of the mutant AHR^{nls} protein, we translated the cDNA in a reticulocyte lysate system. To demonstrate that the mutant receptor bound ligand normally, we performed labeling experiments with the photoaffinity ligand 2-azido-3-[¹²⁵I]iodo-7,8-dibromodibenzo-*p*-dioxin. We observed

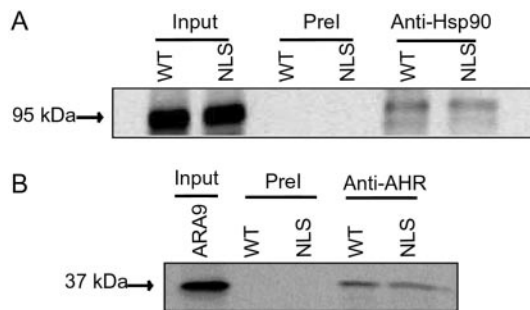


FIG. 2. Capacity of AHR^{nls} to form complexes with HSP90 and ARA9. *A*, co-immunoprecipitation of AHR^{nls} with HSP90. Five microliters of *in vitro* translated [³⁵S]methionine-labeled wild type AHR or AHR^{nls} was incubated with 2 μ g of anti-HSP90 antibody and precipitated with Protein A-Sepharose. Reticulocyte lysates contain large amounts of HSP90, so no additional protein is added. *B*, co-immunoprecipitation of ARA9 with AHR^{nls}. Five microliters of *in vitro* translated [³⁵S]methionine-labeled full-length ARA9 was incubated with either wild type AHR or AHR^{nls}. Protein complexes were incubated with 2 μ g of the AHR-specific antibody and precipitated using Protein A-Sepharose. All proteins in *A* and *B* were eluted from Protein A-Sepharose and separated by SDS-PAGE gels and visualized by autoradiography. *Input*, a loading control representing 100% of the radiolabeled ARA9 used in the assay. *Prel*, the preimmune control.

that the mutant receptor bound this ligand with a capacity that was similar to the wild-type protein (Fig. 1*B*). To determine the DNA binding capacity of the AHR^{nls} protein, we performed gel shift analysis with a consensus DRE oligonucleotide (Fig. 1*C*). In the absence of agonists and in the absence or presence of ARNT, neither the AHR nor the AHR^{nls} proteins interacted significantly with a ³²P-labeled DRE oligonucleotide. The addition of the agonist β NF induced formation of the wild-type recombinant AHR·ARNT·DRE complex that could be blocked by the addition of the anti-AHR antibody. However, the addition of β NF failed to induce formation of a recombinant AHR^{nls}/ARNT/DRE complex, indicating that DNA binding is disrupted by the amino acid replacements (Fig. 1*C*).

We used indirect immunofluorescence to determine the influence of the NLS mutation on the subcellular localization of the AHR in mammalian cells. In order to perform this experiment in the absence of endogenous wild-type AHR, we generated "immortalized" fibroblasts from *Ahr*^{-/-} embryos using a 3T3 protocol (32). The *Ahr*^{-/-} fibroblasts were transiently transfected with AHR or AHR^{nls} cDNAs (pTgTAHRT7 or pSV-AHR^{nls}, respectively). Following treatment with either vehicle or 1 nM TCDD, cells were fixed, and the localization of the AHR or AHR^{nls} protein was visualized using anti-AHR antibody and a fluorescein isothiocyanate-conjugated secondary antibody. We observed that wild-type AHR localizes to the cytosol in untreated fibroblasts but moves to the nucleus within 2 h after treatment of cells with 1 nM TCDD, (Fig. 1, *D* and *E*). As predicted, the AHR^{nls} protein was constitutively cytoplasmic, and its localization was not affected by TCDD (Fig. 1, *F* and *G*). This block in nuclear localization was also observed in COS7 and murine hepatoma cells (data not shown).

To demonstrate the capacity of the AHR^{nls} protein to form normal complexes with its cognate cytosolic chaperones, we performed coimmunoprecipitation experiments with HSP90 and ARA9. For these experiments, proteins were expressed *in vitro* in reticulocyte lysate. For interaction analysis with HSP90, ³⁵S-labeled AHR or AHR^{nls} were immunoprecipitated with antibodies to HSP90 (Fig. 2*A*). For interaction analysis with ARA9, ³⁵S-labeled ARA9 was incubated in the presence of unlabeled AHR and AHR^{nls} and precipitated with anti-AHR antibody (Fig. 2*B*). Results from three independent experiments indicated that both the AHR and AHR^{nls} proteins formed complexes with the chaperones ARA9 and HSP90 with

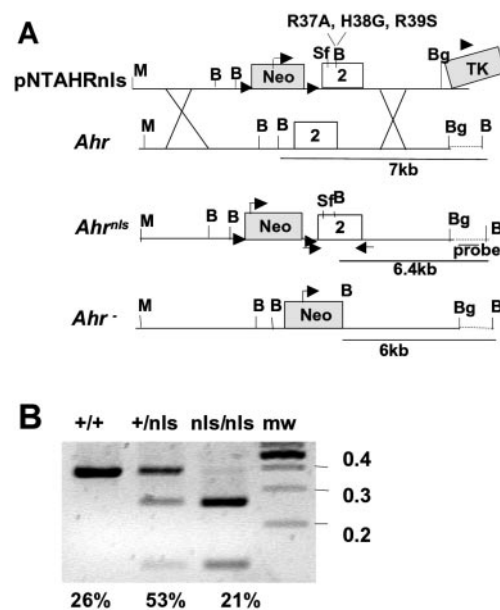


FIG. 3. Gene targeting of pNTAHR^{nls} to the germ line in mice. *A*, schematic of targeting construct and resulting alleles. The pNTAHR^{nls} targeting construct is depicted at the top, indicating positions of exon 2, the neomycin resistance gene cassette (*Neo*), the herpes simplex virus thymidine kinase cassette (*TK*), and informative restriction sites (*Mlu* (*M*), *Bam*HI (*B*), *Bgl*II (*Bg*), *Srf*I (*Sf*)). Amino acid replacements are depicted above. Below the targeting construct are wild type allele (*Ahr*⁺) and the resulting mutant allele (*Ahr*^{nls}). The *Ahr*-null allele (*Ahr*⁻) is included for comparison. Below each are lengths of diagnostic *Bam*HI fragments for Southern genotyping. Locations of probe and primers used for genotyping in ES cells and mice are shown below the *Ahr*^{nls} allele. *B*, representative PCR genotyping results. Primers amplify the 380-bp wild type *Ahr*⁺ allele. Product is cut into 140- and 240-bp fragments by *Bam*HI after amplification of the *Ahr*^{nls} allele. Genotype is listed above each representative lane, and the percentage of animals of each genotype recorded at weaning is noted below each lane (*n* = 86). *MW*, 100-bp ladder molecular weight marker.

similar capacity. The results from representative experiments are shown in Fig. 2. Together these results indicate that AHR^{nls} is capable of interacting with both HSP90 and ARA9 in a manner similar to the wild type AHR yet is no longer capable of translocating to the nucleus and interacting with DNA at DRE elements (Figs. 1 and 2).

Generation of Ahr^{nls/nls} Mice and Their Controls—To generate mice with mutant AHR^{nls} protein, we used PCR to alter the above mentioned sequences of the basic region of AHR (exon 2) in a 15-kb region of homologous genomic DNA from the *Ahr* locus (Fig. 3*A*). The targeting construct was designed to insert the neomycin cassette into a similar region of *Ahr* as was done previously to generate the null mutation (*Ahr*^{-/-}) (7). After selection in both G418 and Ganciclovir, surviving clones were screened by Southern blot, and correctly targeted clones were used to generate chimeras and ultimately germ line transmission of the AHR^{nls} mutation to mice. A representative map of the resulting *Ahr*^{nls} allele is depicted in Fig. 3*A* beside the *Ahr*^{-/-} allele and wild type alleles. The resulting *Ahr*^{nls/nls} mice (formal genetic designation *Ahr*^{tmBra2}) are born at a frequency consistent with a nonlethal allele, and the animals are fertile (Fig. 3*B* and data not shown).

Characterization of Ahr^{nls} Mutation in Vivo—Expression levels of each mutant AHR protein were determined by Western blot and photoaffinity labeling of receptor from liver protein extracts. Visual inspection of the Western blots suggested that the expression of receptor from the *Ahr*^{nls/nls} mouse liver was approximately equivalent to that observed in the *Ahr*^{+/-} liver. Both of these samples expressed the receptor at a level that

was approximately one-half of what we observed from the *Ahr*^{+/+} mouse liver (Fig. 4A). Since Western blots are a semi-quantitative method, we provided an independent and more quantitative assessment of AHR expression levels by photoaffinity labeling the receptors with increasing amounts of the ligand 2-azido-3-[¹²⁵I]iodo-7,8-dibromodibenzo-*p*-dioxin (Fig. 4B). To quantitate bound photoaffinity ligand in the 104-kDa AHR bands, excised radioactive gel slices were quantified in a γ counter. In keeping with what we observed based upon Western blots, we found that the level of functional binding sites for this ligand in liver extracts of *Ahr*^{nls/nls} mice approximated the levels found in *Ahr*^{+/-} animals and was half of the level found in *Ahr*^{+/+} mice (Fig. 4B). In an effort to determine whether the ligand binding affinity was the same for receptor found in *Ahr*^{+/-} and *Ahr*^{nls/nls} mice, we generated a saturation binding isotherm with increasing amounts of radioligand. A modified Scatchard analysis of the binding data revealed similar affinities between wild-type AHR and AHR^{nls} proteins derived from liver cytosols (Fig. 4, C and D). As a result of these findings, we included heterozygous *Ahr*^{+/-} mice as controls in most experiments.

To determine whether the mutant AHR protein signals *in vivo*, *Ahr*^{nls/nls}, *Ahr*^{+/+}, and *Ahr*^{+/-} animals were injected intraperitoneally with 100 μ g/kg TCDD. After 6 days, liver microsomes were isolated and analyzed for EROD activity. Microsomes from wild type and *Ahr*^{+/-} mice show a similar basal EROD activity that was induced nearly 1000-fold by TCDD (Fig. 4E). In contrast, microsomes from *Ahr*^{nls/nls} mice showed only basal EROD activity that was not altered by TCDD treatment. This result indicates that the AHR^{nls} protein cannot activate gene transcription from DRE elements *in vivo*.

***Ahr*^{nls/nls} Mice Are Resistant to TCDD Toxicity**—To determine whether the NLS mutation influenced the role of the AHR in the toxicological response to TCDD, we exposed male *Ahr*^{nls/nls}, *Ahr*^{-/-}, *Ahr*^{+/-}, and *Ahr*^{+/+} mice to TCDD and measured liver hypertrophy and thymic involution, two highly reproducible end points associated with TCDD toxicity in animals. Male, 5–6-week-old animals were treated with 100 μ g/kg TCDD in *p*-dioxane or an equivalent volume of *p*-dioxane alone. Mice were sacrificed 6 days later, and liver and thymus wet weights were recorded. Liver weights in *Ahr*^{+/+} and *Ahr*^{+/-} animals increased significantly in response to TCDD, yet neither the *Ahr*^{-/-} and *Ahr*^{nls/nls} animals showed any TCDD-induced increase in liver weights in response to TCDD (Fig. 5A, $p \leq 0.05$). In addition, we observed that the relative liver weights of both the *Ahr*^{nls/nls} and the *Ahr*^{-/-} mice were reduced $\sim 28\%$ as compared with the *Ahr*^{+/+} or *Ahr*^{+/-} controls ($p \leq 0.05$; Fig. 5A). Thymus weights in *Ahr*^{+/+} and *Ahr*^{+/-} animals decreased significantly in response to TCDD, yet *Ahr*^{-/-} and *Ahr*^{nls/nls} animals did not show any significant TCDD-induced decreases in thymus weights ($p \leq 0.05$; Fig. 5B). In this experiment, there was a trend suggesting that TCDD might have a subtle influence on relative thymus weights of *Ahr*^{-/-} and *Ahr*^{nls/nls} mice, but independent experiments did not support this relationship (data not shown).

We also examined the closure of palatal shelves in an organ culture model system, where we can directly expose the tissue to TCDD (36, 37). Palates were excised from embryonic day 12.5 *Ahr*^{+/+}, *Ahr*^{+/-}, and *Ahr*^{nls/nls} embryos, and the tissue was directly exposed to TCDD in culture for 4 days. In response to 0.03% (v/v) Me₂SO alone, genotype did not affect palatal closure. However, when exposed to 3 nM TCDD in Me₂SO, no palates from *Ahr*^{+/+} or *Ahr*^{+/-} mice fused, whereas the TCDD-exposed palates from *Ahr*^{nls/nls} animals all fused (Table I). This result was not different from Me₂SO-treated controls. Therefore, AHR^{nls} protein fails to activate those events, leading to

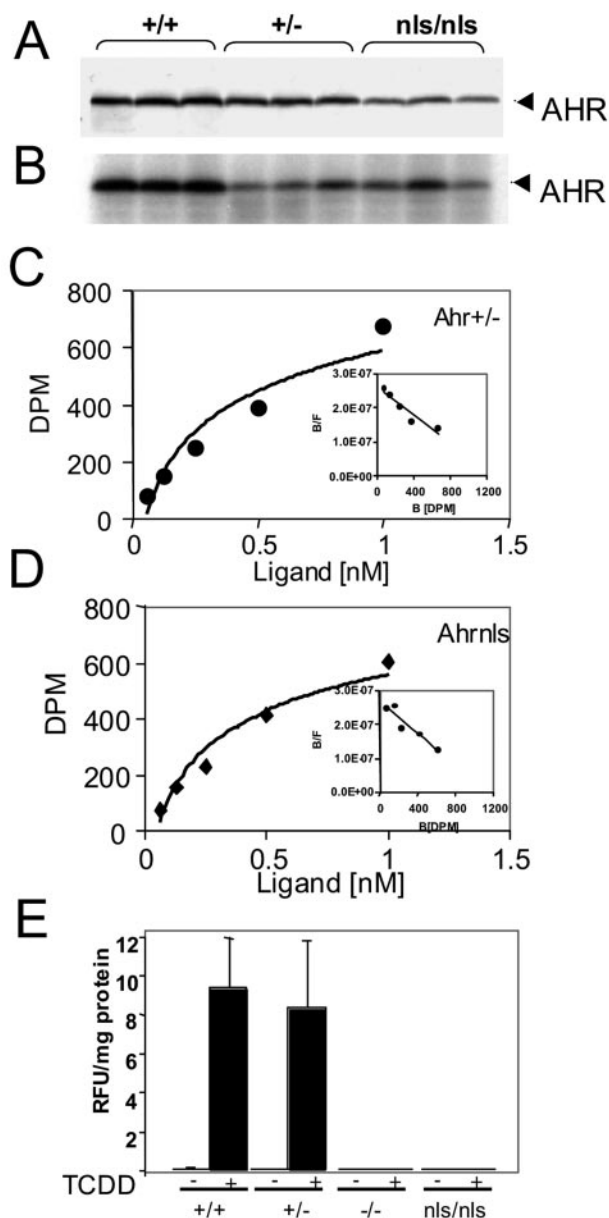


FIG. 4. The AHR^{nls} protein binds ligand but does not activate DRE-mediated transcription *in vivo*. A, Western blot analyses showing protein levels in liver cytosolic extracts from three individual animals from each genotype *Ahr*^{+/+}, *Ahr*^{+/-}, and *Ahr*^{nls/nls}. Cytosolic protein (150 μ g) is loaded in each well of a 7.5% polyacrylamide gel. Visualization is performed with anti-AHR antibody. B, ligand binding capacity of cytosolic AHR proteins using 1 nM photoaffinity ligand. 150 μ g of the same protein extracts in A were incubated with [¹²⁵I]Br₂DpD and activated at 310-nm light. Samples were washed to remove unbound ligand and separated by SDS-PAGE. Ligand binding was analyzed by autoradiography. C and D, ligand binding of the AHR from *Ahr*^{+/-} and *Ahr*^{nls/nls} animals. Cytosolic extracts from *Ahr*^{+/-} (C) and *Ahr*^{nls/nls} (D) animals were incubated with increasing amounts of [¹²⁵I]Br₂DpD ligand. Saturation binding isotherms are plotted as a function of total ligand versus bound (dpm counted from excised gel pieces). Each point on the plot represents the average of two experiments. Insets, Scatchard analysis of binding data calculated according to "Experimental Procedures." B_{\max} values are expressed as relative dpm: *Ahr*^{+/-} $B_{\max} = 1290$; *Ahr*^{nls/nls} $B_{\max} = 1110$. Because of significant overlap between curves and for clarity, results from *Ahr*^{+/-} (C) and *Ahr*^{nls/nls} (D) are plotted separately. E, EROD activity analyses from microsomes in *Ahr*^{+/+}, *Ahr*^{+/-}, *Ahr*^{-/-}, and *Ahr*^{nls/nls} animals. Microsomal isolations from liver extracts were incubated with ethoxyresorufin in the presence of NADPH. EROD activity was measured from *p*-dioxane-treated (-) and *p*-dioxane plus TCDD-treated (+) animals at excitation of 510 nm and emission of 590 nm. Fluorescent values were normalized to total protein levels. Error bars, S.D. values from three individual animals.

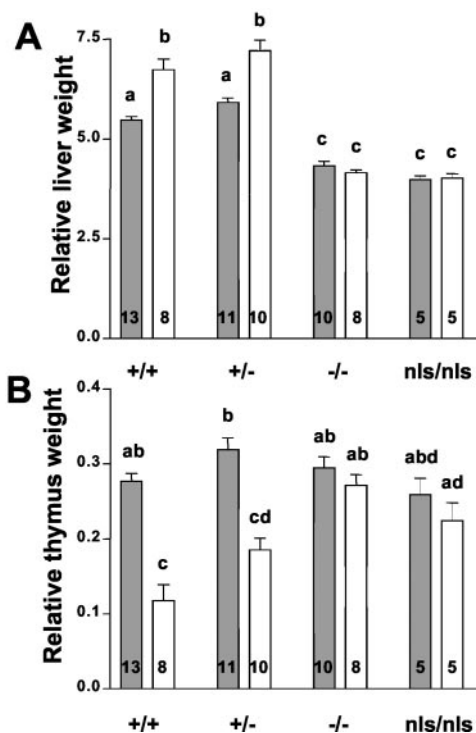


FIG. 5. Comparison of toxicity of TCDD measured in liver and thymus in $Ahr^{+/+}$, $Ahr^{+/-}$, $Ahr^{-/-}$, and $Ahr^{nls/nls}$ animals. Animals 5 weeks old were exposed by intraperitoneal injection to a single 100 $\mu\text{g}/\text{kg}$ dose TCDD dissolved in *p*-dioxane (vehicle) or equivalent volume of *p*-dioxane alone. After 6 days, liver (A) and thymus (B) were excised and weighed and normalized to total body weight. Gray bars, vehicle-treated animals; white bars, TCDD-treated animals. Error bars, S.D. The number of animals used in each group is noted within each bar. Those groups not sharing a superscript letter differ significantly at $p \leq 0.05$.

TABLE I
Closure in wild type and mutant palates following direct exposure to TCDD in organ culture

Primary and secondary palatal shelves were dissected from embryonic day 12.5 animals and cultured in media containing either 0.03% Me_2SO alone or 3 nM TCDD in 0.03% Me_2SO for 4 days. Palatal shelves were scored as “fused” if fused along entire length of shelf at the end of the 4 days. Ambiguous partial fusion events occurred occasionally and were not included.

Genotype	Me_2SO		TCDD	
	Fused	Not fused	Fused	Not fused
$Ahr^{+/+}$	11	0	0	9
$Ahr^{+/-}$	9	0	0	20
$Ahr^{nls/nls}$	3	0	13	0

cleft palate formation in response to TCDD.

$Ahr^{nls/nls}$ Mice Show Developmental Defects Similar to $Ahr^{-/-}$ Mice—Wild type and $Ahr^{nls/nls}$ animals were examined for developmental phenotypes that have been previously reported in $Ahr^{-/-}$ mice (6–8, 10, 39–43). Tissue wet weights were measured on major organs of 8-week-old male mice. We observed that relative liver weights in $Ahr^{nls/nls}$ animals were 27% smaller when compared with $Ahr^{+/+}$ controls (Fig. 6A; $p \leq 0.001$). The reduced $Ahr^{nls/nls}$ liver weights were identical to those reported previously in $Ahr^{-/-}$ animals (7). Also similar to what has been reported for $Ahr^{-/-}$ animals, normalized spleen and heart weights were moderately increased in $Ahr^{nls/nls}$ compared with $Ahr^{+/+}$ (Fig. 6, B and C; $p \leq 0.001$). Importantly, relative weights of thymus, kidney, lung, testes, and brain remained unaffected by genotype (thymus weight is shown as an example) (Fig. 6D).

In $Ahr^{-/-}$ mice, the DV remains open throughout adulthood.

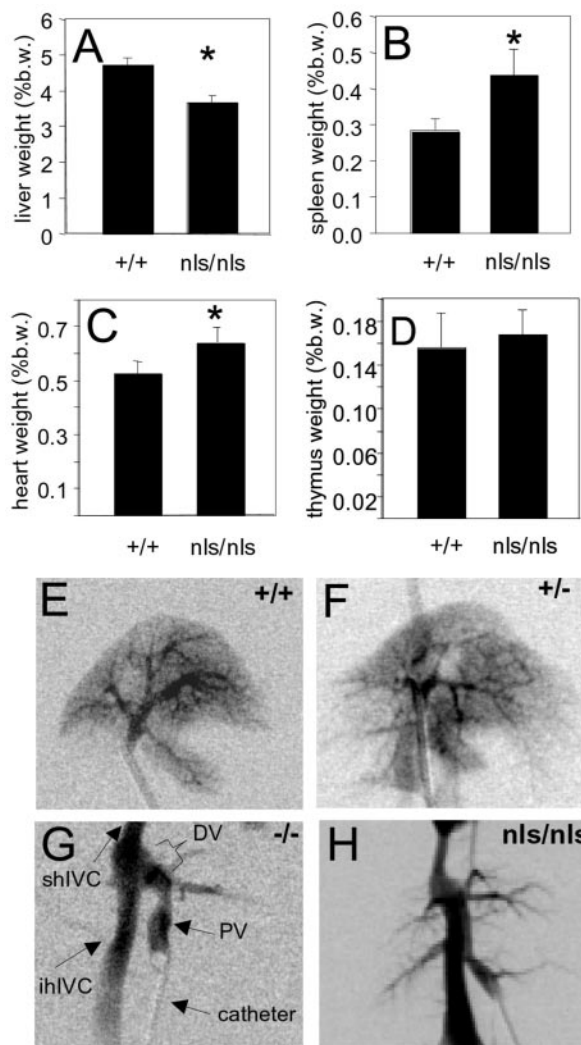


FIG. 6. Developmental phenotype of the $Ahr^{nls/nls}$ mouse. Weights of excised organs from 8-week-old animals were normalized to body weight (b.w.). Left bar, $Ahr^{+/+}$; right bar, $Ahr^{nls/nls}$. A, liver; B, spleen; C, heart; D, thymus. Error bars, S.D. of at least four animals. Statistical differences are noted by a star ($p \leq 0.001$). E–H, radiographs of portal vein-injected contrast agent in animals. E, $Ahr^{+/+}$; F, $Ahr^{+/-}$; G, $Ahr^{-/-}$; H, $Ahr^{nls/nls}$. The arrows in G indicate key features. PV, portal vein; shIVC, suprahepatic inferior vena cava; ihIVC, infrahepatic inferior vena cava. Representative images were taken ~ 10 s after injection of contrast agent. G and H are enlarged $\sim 2\times$ the size of E and F for labeling clarity.

To determine whether a similar phenotype exists in $Ahr^{nls/nls}$ animals, we performed time lapse angiography to observe the flow of contrast medium through the perfused liver. In the control $Ahr^{+/+}$ and $Ahr^{+/-}$ animals, contrast medium flowed into the portal vein and immediately into the portal branches of the liver vasculature (Fig. 6, E and F, respectively). After filling the major branching veins of the liver, contrast entered the suprahepatic IVC and then filled the infrahepatic IVC. However, contrast medium in $Ahr^{nls/nls}$ mice flowed directly from the portal vein to the IVC. The shunt between the portal vein and the IVC was clearly visible as a short segment that runs perpendicular to both the portal vein and IVC within the liver (Fig. 6H). This vascular pattern is consistent with patent DV in $Ahr^{-/-}$ mice (Fig. 6G and Ref. 10)

DISCUSSION

Previous cell culture and *in vitro* analyses of AHR signaling have provided a detailed picture of the mechanism by which the ligand-activated AHR up-regulates the expression of certain

XMEs through receptor-DRE interactions within the nucleus (44). However, this understanding of the DRE-linked transcriptional targets of AHR has not yet explained the variety of toxic events that occur in response to potent agonists like TCDD; nor have they been used to explain the aberrant liver/vascular development observed in *Ahr*^{-/-} mice. Although it may be simple to assume that these receptor dependent processes are related to DRE-driven transcription, several reports have suggested that the AHR may signal through DRE-independent pathways (11, 13–16, 17, 45, 46, 48). Thus, we are still in need of a formal proof to demonstrate that the mechanism by which XMEs are up-regulated is similar to the mechanism by which the AHR plays a role in TCDD toxicity or regulates aspects of mammalian development.

In an effort to better understand the importance of DRE-independent signaling, we are constructing mutant mouse models that directly test the roles of receptor functional domains on various aspects of AHR biology *in vivo*. The AHR^{nls} mouse was designed specifically to examine the role that cytosolic events play in TCDD-induced toxicity and AHR-dependent liver development. In this endeavor, we chose to first generate animals with an AHR protein that can be activated by ligand but that is not capable of translocating to the nucleus or binding to DREs. The rationale for such a model is that it can be used to identify AHR-mediated end points that do not require nuclear localization of the AHR. Put another way, with this model we may be able to identify cytosolic signaling pathways related to AHR biology, or we can provide evidence to refute their existence.

Generation of this mouse model required consideration of the overlapping domain structure of the basic α -helix of AHR within the bHLH domain. This basic region encodes the nuclear localization motif that is revealed upon ligand binding, and it harbors the DRE contact residues by which the AHR interacts with its DNA half-site within these enhancers (20, 28). In early characterization studies, we demonstrated that the NLS mutation resulted in an AHR protein that interacts normally with chaperones but that could not translocate to the nucleus or bind to DREs upon exposure to agonists. To this end, we used immunocytochemistry to demonstrate that the mutant protein remained cytosolic in the presence of an agonist. We then also used a battery of *in vitro* assays to demonstrate that the mutant protein was capable of interactions with its chaperones HSP90 and ARA9 (Figs. 1 and 2). Once the predicted consequences of our mutations were confirmed, we used homologous recombination in ES cells to replace the endogenous bHLH region of the *Ahr* locus (exon 2) with a mutated exon carrying the NLS amino acid substitutions.

There are two major points regarding controls that arose during the course of these experiments. The first relates to genetic background. Because embryonic stem cells are derived from 129Sv mice that carry the d allele of *Ahr*, we utilized the C57BL/6-*Ahr*^d animals for backcrossing and to generate control animals for these experiments. Mice harboring the wild-type d allele are not used as frequently as those strains harboring the more common b alleles due to the fact that the d allele encodes a receptor with a lower binding affinity for TCDD (49). Importantly, this lower binding affinity exhibited by the d allele has been shown to be similar to the human AHR and thus may serve as a more relevant model for human toxicity (47). The major influence this parental allele had on our experimental design was that it necessitated the development of dosing protocols that would induce toxic end points in mice harboring this lower affinity receptor. Thus, it will be noted that the doses of TCDD used in these studies are about 5–10-fold higher than are commonly used in most mouse studies.

The second point relevant to control animals is that although the AHR from the d allele and the nls allele display similar affinities for ligand, the nls allele is expressed at a lower level (Fig. 4). Our photoaffinity labeling of the AHR found in the livers of *Ahr*^{nls/nls} mice indicated that the mutant protein was expressed at a level that was approximately one-half of that observed in *Ahr*^{+/+} mice. Fortunately, AHR expression in wild-type animals appears to be a direct function of gene copy number.² Therefore, mice that were heterozygous for the d allele and the null allele served as controls (*i.e.* *Ahr*^{+/-}).

To determine whether nuclear events were required for the role of AHR in TCDD toxicity or normal liver development, we performed a number of toxicology experiments with the *Ahr*^{nls/nls} mice. First, we examined the toxic response of the *Ahr*^{nls/nls} mice by injecting the animals with TCDD and assaying for liver hypertrophy and thymic involution. We found that *Ahr*^{nls/nls} mice failed to exhibit these obvious liver and thymic end points, whereas the corresponding *Ahr*^{+/+} and *Ahr*^{+/-} controls were quite sensitive (Fig. 5, A and B). We also examined a TCDD-induced teratogenic response, namely the formation of cleft palate. To this end, we exposed embryonic day 12.5 palatal shelves directly to TCDD in culture. This protocol directly exposes palate tissue in culture to TCDD and eliminates issues related to maternal influence. Just like the hepatic and thymic responses, we observed that the palates from *Ahr*^{nls/nls} animals were completely resistant to TCDD exposure, whereas the corresponding controls were sensitive (Table I). From these results, we conclude that nuclear localization is required for TCDD-induced liver hypertrophy, thymic atrophy, and cleft palate formation.

We also assessed the role of cytosolic events in the developmental aspects of AHR biology. In this regard, all of the known developmental defects we have previously observed in *Ahr*^{-/-} mice are also observed in the *Ahr*^{nls/nls} mice. To this point, the *Ahr*^{nls/nls} mice display a similar reduction in relative liver weight and moderate increases in heart and spleen weights. In more recent experiments, we have also observed that the livers of *Ahr*^{nls/nls} display microvesicular fatty changes around day 6 after birth (7). Just as in the null allele these fatty changes resolve by adulthood (data not shown). Finally, the presence of a patent DV was observed in both the *Ahr*^{nls/nls} mice and in the *Ahr*^{-/-} mice (Fig. 6). Just as in the toxicology experiments described above, we are led to conclude that the nuclear localization of the AHR is an essential step in the receptor pathways that regulate liver development/DV closure.

The *Ahr*^{nls/nls} mice provided us with a model system to test the importance of cytosolic interactions in certain aspects of AHR biology. Given that it would be impossible to test each proposed model in our system (*i.e.* cSrc, ceramide, etc.), our strategy was to carry out experiments that would examine the relative importance of cytosolic *versus* nuclear signaling with regard to a few classic receptor-mediated end points (*i.e.* liver hypertrophy, thymic involution, cleft palate formation, and persistence of the DV). Although our results are not supportive of a role for cytosolic events for these end points, it is still possible that cytosolic signaling by the AHR is important in end points not examined here (*e.g.* chloracne, altered T-cell responses, etc.). It is also important to point out that we cannot rule out the possibility that cytosolic signaling does occur and that it is dependent upon the exact identity of residues Arg³⁷, His³⁸, and Arg³⁹. In an effort to address such possibilities, we plan to make this mutant available to any laboratory interested in formally examining the influence of the nls allele on

² M. K. Bunger, S. M. Moran, E. Glover, T. L. Thomae, G. P. Lahvis, B. C. Lin, and C. A. Bradfield, unpublished observation.

any proposed cytosolic mechanism. Finally, given that the NLS mutation eliminates nuclear localization, it remains possible that nuclear, yet non-DRE binding events are important in AHR biology. Nuclear events such as cross-talk with the hypoxia-inducible factor and interactions with steroid receptors are still potentially important mechanisms of TCDD action or AHR-mediated developmental signaling.

Acknowledgments—We acknowledge members of the University of Wisconsin-Madison Transgenic Animal Facility for expert technical assistance.

REFERENCES

- Nebert, D. W., and Gonzalez, F. J. (1987) *Annu. Rev. Biochem.* **56**, 945–993
- Hankinson, O. (1995) *Annu. Rev. Pharmacol. Toxicol.* **35**, 307–340
- Schmidt, J. V., and Bradfield, C. A. (1996) *Annu. Rev. Cell Dev. Biol.* **12**, 55–89
- Whitlock, J. P., Jr., Chichester, C. H., Bedgood, R. M., Okino, S. T., Ko, H. P., Ma, Q., Dong, L., Li, H., and Clarke-Katzenberg, R. (1997) *Drug Metab. Rev.* **29**, 1107–1127
- Poland, A., and Knutson, J. C. (1982) *Annu. Rev. Pharmacol. Toxicol.* **22**, 517–554
- Fernandez-Salguero, P. M., Hilbert, D. M., Rudikoff, S., Ward, J. M., and Gonzalez, F. J. (1996) *Toxicol. Applied Pharmacol.* **140**, 173–179
- Schmidt, J. V., Su, G. H.-T., Reddy, J. K., Simon, M. C., and Bradfield, C. A. (1996) *Proc. Natl. Acad. Sci. U. S. A.* **93**, 6731–6736
- Fernandez-Salguero, P. M., Ward, J. M., Sundberg, J. P., and Gonzalez, F. J. (1997) *Vet. Pathol.* **34**, 605–614
- Mimura, J., Yamashita, K., Nakamura, K., Morita, M., Takagi, T. N., Nakao, K., Emak, M., Sogawa, K., Yasuda, M., Katsuki, M., and Fujii-Kuriyama, Y. (1997) *Genes Cells* **2**, 645–654
- Lahvis, G., Lindell, S., Thomas, R., McCuskey, R., Murphy, C., Glover, E., Bentz, M., Southard, J., and Bradfield, C. (2000) *Proc. Natl. Acad. Sci. U. S. A.* **97**, 10442–10447
- Enan, E., and Matsumura, F. (1996) *Biochem. Pharmacol.* **52**, 1599–1612
- Blankenship, A., and Matsumura, F. (1997) *Mol. Pharmacol.* **52**, 667–675
- Klinge, C. M., Kaur, K., and Swanson, H. I. (2000) *Arch. Biochem. Biophys.* **373**, 163–174
- Ge, N.-L., and Elferink, C. J. (1998) *J. Biol. Chem.* **273**, 22708–22713
- Puga, A., Barnes, S. J., Dalton, T. P., Chang, C., Knudsen, E. S., and Maier, M. A. (2000) *J. Biol. Chem.* **275**, 2943–2950
- Chan, W. K., Yao, G., Gu, Y. Z., and Bradfield, C. A. (1999) *J. Biol. Chem.* **274**, 12115–12123
- Gradin, K., McGuire, J., Wenger, R. H., Kvietikova, I., fhitelaw, M. L., Toftgard, R., Tora, L., Gassmann, M., and Poellinger, L. (1996) *Mol. Cell. Biol.* **16**, 5221–5231
- Fukunaga, B. N., and Hankinson, O. (1996) *J. Biol. Chem.* **271**, 3743–3749
- Eguchi, H., Ikuta, T., Tachibana, T., Yoneda, Y., and Kawajiri, K. (1997) *J. Biol. Chem.* **272**, 17640–17647
- Ikuta, T., Eguchi, H., Tachibana, T., Yoneda, Y., and Kawajiri, K. (1998) *J. Biol. Chem.* **273**, 2895–2904
- Bacsi, S. G., and Hankinson, O. (1996) *J. Biol. Chem.* **271**, 8843–8850
- Dong, L., Ma, Q., and Whitlock, J. P., Jr. (1996) *J. Biol. Chem.* **271**, 7942–7948
- Swanson, H. I., and Yang, J. H. (1996) *J. Biol. Chem.* **271**, 31657–31665
- Dolwick, K. M., Swanson, H. I., and Bradfield, C. A. (1993) *Proc. Natl. Acad. Sci. U. S. A.* **90**, 8566–8570
- Carver, L. A., LaPres, J. J., Jain, S., Dunham, E. E., and Bradfield, C. A. (1998) *J. Biol. Chem.* **273**, 33580–36159
- Jain, S., Dolwick, K. M., Schmidt, J. V., and Bradfield, C. A. (1994) *J. Biol. Chem.* **269**, 31518–31524
- Carver, L. A., and Bradfield, C. A. (1997) *J. Biol. Chem.* **272**, 11452–11456
- Swanson, H. I., Chan, W. K., and Bradfield, C. A. (1995) *J. Biol. Chem.* **270**, 26292–26302
- LaPres, J. J., Glover, E., Dunham, E. E., Bunger, M. K., and Bradfield, C. A. (2000) *J. Biol. Chem.* **275**, 6153–6159
- Bradfield, C. A., Kende, A. S., and Poland, A. (1988) *Mol. Pharmacol.* **34**, 229–237
- Poland, A., Glover, E., Ebetino, F. H., and Kende, A. S. (1986) *J. Biol. Chem.* **261**, 6352–6365
- Torodo, G. J., and Green, H. (1963) *J. Cell Biol.* **17**, 299–313
- Schmidt, J. V., Carver, L. A., and Bradfield, C. A. (1993) *J. Biol. Chem.* **268**, 22203–22209
- Tybulewicz, V. L. J., Crawford, C. E., Jackson, P. K., Bronson, R. T., and Mulligan, R. C. (1991) *Cell* **65**, 1153–1163
- Poland, A., and Glover, E. (1980) *Mol. Pharmacol.* **17**, 86–94
- Taya, Y., O’Kane, S., and Ferguson, M. W. (1999) *Development* **126**, 3869–3879
- Pisano, M. M., and Greene, R. M. (2000) *Methods Mol. Biol.* **137**, 267–274
- Devore, J., and Peck, R. (1986) *Statistics: The Exploration and Analysis of Data*, West Publishing Co., New York
- Lahvis, G. P., and Bradfield, C. A. (1998) *Biochem. Pharmacol.* **56**, 781–787
- Gonzalez, F. J., and Fernandez-Salguero, P. (1998) *Drug Metab. Dispos.* **26**, 1194–1198
- Peters, J. M., Narotsky, M. G., Elizondo, G., Fernandez-Salguero, P. M., Gonzalez, F. J., and Abbott, B. D. (1999) *Toxicol. Sci.* **47**, 86–92
- McDonnell, W. M., Chensue, S. W., Askari, F. K., Moseley, R. H., Fernandez-Salguero, P., Gonzalez, F. J., and Ward, J. M. (1996) *Science* **271**, 223–224
- Zaher, H., Fernandez-Salguero, P. M., Letterio, J., Sheikh, M. S., Fornace, A. J., Roberts, A. B., and Gonzalez, F. J. (1998) *Mol. Pharmacol.* **54**, 313–321
- Whitlock, J. P., Jr. (1999) *Annu. Rev. Pharmacol. Toxicol.* **39**, 103–125
- Dunlap, D. Y., Ikeda, I., Nagashima, H., Vogel, C., and Matsumura, F. (2002) *Toxicology* **172**, 125–141
- Reiners, J. J., Jr., and Clift, R. E. (1999) *J. Biol. Chem.* **274**, 2502–2510
- Ema, M., Ohe, N., Suzuki, M., Mimura, J., Sogawa, K., Ikawa, I., and Fujii-Kuriyama, Y. (1994) *J. Biol. Chem.* **269**, 27337–27343
- Tian, Y., Ke, S., Denison, M. S., Rabson, A. B., and Gallo, M. A. (1999) *J. Biol. Chem.* **274**, 510–515
- Okey, A. B., Vella, L. M., and Harper, P. A. (1989) *Mol. Pharmacol.* **35**, 823–830